Journal of Applied Fluid Mechanics, Vol. 7, No. 3, pp. 525-534, 2014.
Available online at www.jafmonline.net, ISSN 1735-3572, EISSN 1735-3645.

Experimental Investigation of "Why an AC Dielectric Barrier Discharge Plasma Actuator is Preferred to DC Corona Wind Actuator in Boundary Layer Flow Control?"

G. Tathiri[†1], E. Esmaeilzadeh[2], S. M. Mirsajedi[3] and H. Mahdavi Moghaddam[1]

[1] *Department of Mechanical and Aerospace Engineering, Science and Research Branch, Islamic Azad University, Tehran, Iran*
[2] *Heat & Fluid Research Laboratory, Department of Mechanical Engineering, Tabriz University,Tabriz, Iran*
[3]*Assistant Professor Faculty of New Technologies EngineeringShahid Beheshti University Tehran, Iran*

† Corresponding Author Email*: gh_tathiri@iauz.ac.ir*

(Received June 10, 2013; accepted November 3, 2013)

ABSTRACT

In this paper, characteristics of the flow induced in the boundary layer by an AC-Dielectric Barrier Discharge (DBD) plasma actuator are compared against those of a DC-corona wind actuator. This is achieved by visualization of the induced flow using smoke injection and measuring the horizontal induced velocity. Our measurements show that the maximum induced velocity of an AC-DBD actuator is about one order of magnitude larger than that of a DC-corona actuator. For an AC-DBD actuator, the induced velocity is maximized on the plate surface while for a DC-corona actuator the induced velocity peaks at about 20mm above the surface. Using flow visualization, we demonstrate that the induced velocity of an AC-DBD actuator is parallel to the surface, while the induced velocity of a DC-corona actuator has components perpendicular to surface.

Keywords: Active flow control, AC-DBD, DC-corona, Induced flow.

NOMENCLATURE

$E(t)$	electric field intensity, $kgms^{-3}A^{-1}$	W	electric power consumption of the AC/DC actuator per unit length of electrodes, $kgms^{-3}$
f_{ac}	AC-carrier-frequency of the actuator, s^{-1}	Y	vertical distance from surface, m
$f_b^*(t)$	unsteady body force applied to the particles in the presence of electric field, $kgms^{-2}$	ρ_e	electric charge density, sA
I_{rms}	root-mean-square current intensity, A	ε	permittivity, $kg^{-1}m^{-3}s^4A^2$
L_e	electrode length, m	ρ	air density, kgm^{-3}
U_x	tangential induced velocity, ms^{-1}	ΔV	applied AC/DC voltage, $kgm^2s^{-3}A^{-1}$

1. INTRODUCTION

The methods of flow control in boundary layer can be divided into three groups: (1) passive control, (2) active control and (3) compound control. Passive methods are usually lighter in weight and require less energy to operate. However, they have the disadvantage that by changing the flow conditions (Reynolds number, angle of attack, etc.) their performance may easily be altered or lost. Because of these reasons, nowadays the active methods are more desirable than passive methods.

Among the active flow control methods, in the past decade, Electro-Hydro-Dynamic (EHD) actuators have gained special attention. These actuators ionize the air and add a localized momentum to the flow through a collision of the migrating charged particles with the neutral species of the air. A number of different plasma actuators have been considered for controlling fluid flow phenomena, including dielectric barrier discharge (DBD) (Corke et al., 2004; Roth, 2003), dc glow discharge

(Kimmel *et al.*, 2004), radio-frequency glow discharge (Merriman *et al.*, 2001), and filamentary arc discharge (Samimy *et al.*, 2004). Suchomel *et al.*, (2003) provide an overview of different plasma technologies currently under use for aeronautical applications. The main advantages of the EHD actuators are as follows: no moving parts, a short response time, easy installation, low weight, easy application on the surface without any change in the surface geometry, low power consumption, no need to remove the actuator when they are not in use and a high efficiency in transforming electrical to mechanical energy (Adamo *et al.*, 2002).

Depending on the application, the EHD actuators may be divided into three groups: corona-based devices (Colver *et al.*, 1999; Noger *et al.*, 1997), dielectric barrier discharge (DBD) devices (Roth *et al.*, 2000; Wilkinson, 2003), and plasma sheet devices (Adamo *et al.*, 2002; Artana *et al.*, 2003; Sosa *et al.*, 2004).

In both methods of corona wind and plasma sheet, to avoid the possible electric discharge, the separation distance between the two electrodes has to be large. Therefore the two electrodes cannot be placed closer to each other than a specific limit. This limit depends on the applied voltage and the ambient conditions. Furthermore, in the DC corona discharge regime, because of the collision of ions to the cathode surface, the cathode surface becomes extremely hot to the point of structural breakdown. This reduces the power of ionic wind and its effectiveness on the fluid flow field. Consequently, because of these limitations with the corona wind and plasma sheet methods, the AC-DBD plasma actuators have become more popular in the recent years.

In DBD plasma actuators, since the distance between the electrodes is covered with an insulating material that has high electrical resistance to discharge, the electrodes with a smaller separation distance can be utilized. Thus the intensity of the electric field required for ionization of air molecules increases significantly. Therefore a high-power plasma can be generated to better accelerate the fluid flow. This helps to substantially reduce the size of the actuators and consequently install them in a smaller place and in the exact desired location.

The plasma actuator is one of the newest methods of EHD active flow control which is used for more than a decade. This actuator has various applications including separation control on airfoil leading edge (Post *et al.*, 2004; Benard *et al.*, 2008), control of airfoil dynamic stall (Pose *et al.*, 2006), flow control in bluff bodies (Do *et al.*, 2007; Thomas *et al.*, 2005; Corke *et al.* ,2008; Rizzetta *et al.*, 2008; Gregory *et al.*, 2008), boundary layer flow control (Schatzman *et al.*, 2008; Baughn *et al.*, 2006; Font *et al.*, 2006), high lift-applications (Corke *et al.*, 2004) and turbo-machinery flow control (Huang *et al.*, 2006a, 2006b; Van Ness *et al.*, 2006).

So far, to our knowledge, the AC-DBD methods are preferred to the DC-corona wind actuators in boundary layer flow control over a smooth and flat plate. However, no experimental study has been reported regarding the basic differences between AC-DBD and DC-corona wind actuators. The objective of this paper is to experimentally elaborate "why AC-DBD plasma actuators are preferred to DC-corona actuators in boundary layer flow control?". This is achieved by comparing the characteristics of the induced flow generated by AC and DC actuators.

The experiments are carried out by applying the DC and AC plasma actuators on a flat plate and visualizing their induced flow respectively. The induced flow velocity in the boundary layer is measured by a Pitot tube to compare the magnitude of the induced velocity of the actuators.

2. THEORY OF PLASMA GENERATION

The Electro-Hydro-Dynamic mechanism can create movements to increase the rate of mass transfer in both single-phase and multiphase flows. The effective forces in this mechanism are: (1) Coulomb force (2) de-electro-foretic and (3) electro-striction (Melcher, 1981), which together yield to a total force of:

$$\vec{f}_b^{*}(t) = \rho_e \vec{E}(t) - \frac{1}{2}E^2\nabla\varepsilon + \frac{1}{2}\nabla\left[E^2\rho\left(\frac{\partial\varepsilon}{\partial\rho}\right)\right] \qquad (1)$$

This equation has been derived by Melcher (1981) via a thermodynamics approach and with the assumption that the polarization is a linear function of applied electric field and depends only on the fluid density (ρ). The first term in Eq. (1) is the Coulomb force and is created by the direct injection of free charges by the corona source. The second term is the de-electro-foretic force and is produced by non-homogeneity of the dielectric constant of the material in the interface. The third term is the electro-striction force and is created when the dielectric constant changes with density. A schematic of the three forces are shown in Fig.1 (Seyed-Yagoobi *et al., 1981*), where Fig.1 (a) corresponds to the Coulomb force, (b) is due to the de-electro-foretic, while (c) and (d) correspond to the electro-striction force. Usually, the magnitude of the two last terms in Eq. (1) is negligible in comparison with the first term.

In the corona-based devices, where the input actuation is DC, due to the constant nature of the DC input, the body force is also constant and is always directed from the H.V. electrode to the grounded electrode. On the other hand, in the AC-DBD actuation, due to the oscillating nature of the input AC, the body force is also oscillatory. A sketch of this process is illustrated in Fig. 2 (Corke *et al.*, 2008). In the first half cycle of the actuation, where the exposed electrode is negatively charged, the electrons are emitted from the exposed electrode

and deposited onto the dielectric surface. In the second half cycle of the actuation, where the exposed electrode is positively charged, the deposited electrons on the dielectric surface are emitted from the dielectric surface to the exposed electrode. There is a difference in electron emission in two half cycles. Because of the connectivity of the exposed electrode to an infinite source of electrons (power supply), the rate of electron emission in the first half cycle of actuation is significantly higher than the second half cycle. In the second half cycle only the deposited electrons (on the dielectric surface), which are finite, can emit to the exposed electrode. Due to this asymmetry in the electron emission rate, a net body force is applied to the particles (Corke *et al.*, 2008). This irregularity in two portion of one cycle has been shown by Orlov *et al.*, (2006). This is consistent with the literature for DBD (Gibalov *et al.*, 2000; Pashaie *et al.*, 1994), and was also presented by Enloe *et al.*, (2004).

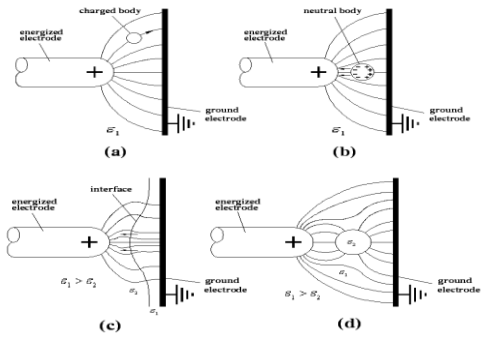

Fig. 1. Three types of electric forces applied to the particles by the electric field. (a) Coulomb, (b) de-electro-foretic, (c) and (d) electro-striction.

In general, triangle waves are more optimal than sine waves, and square waves or rectangular pulses are least favorable in ionizing the air for DBD plasma actuators. Enloe *et al.*, (2004) have shown that a saw-tooth waveform produces more induced thrust in comparison with the sine wave.

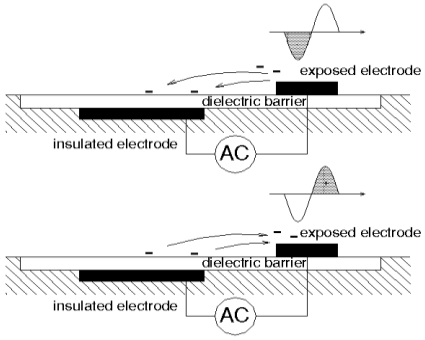

Fig. 2. Illustration of the electron drift that dictates portions of AC period where air ionizes in DBD process.

Based on the formulation of Orlov *et al.*, (2006a, 2006b), the direction of the body force is always from the upper exposed electrode to the lower covered electrode. This is the result of the assumptions in the formulation. In particular, the quasi-equilibrium assumption in which the time scale of the electron and ion is much smaller than the AC carrier frequency. Of course, this is true for electrons, but the case of ions is still the subject of discussion among researchers. Font *et al.*, (2004, 2005) suggested that in the first half cycle, where the electrons are emitted from the upper electrode and positive ions are absorbed to this electrode, the net force is not zero and because of the dominance of ions, is directed towards the upper electrode. In the second half cycle the direction of the electric field is reversed. Due to the force applied from positive ions, which are emitted from the upper electrode, the direction of the resultant force is from the upper electrode to the lower electrode. The magnitude of the body force in the second half cycle is much greater than the first half cycle. Thus the direction of the total net force in one cycle is toward the covered electrode.

The theory suggested by Orlov *et al.*, (2006a, 2006b) is named "push-push" and the theory suggested by Font *et al.*, (2004, 2005) is called "pull-push". The two theories are schematically shown in Fig.3.

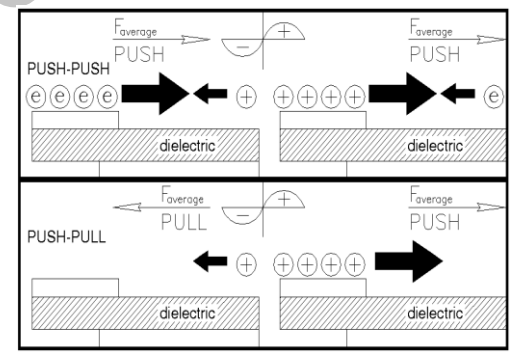

Fig. 3. "push-push" and "pull-push" theory of the AC-DBD plasma.

The experiments of Fort *et al.*, (2006) using photography of the particle direction in one cycle, demonstrated that the tangential force oscillates between two positive values and never becomes zero or negative. This is in agreement with the "push-push" theory of Orlov *et al.*, (2006a, 2006b).

3. EXPERIMENTAL STUDY

For this research, two stages of experiments have been considered:

- Observing the generated DC-corona wind and the AC-DBD plasma by photography in the dark room and visualizing the induced velocity of both actuators by smoke injection technique.

- Measuring the magnitude of the induced velocity of the actuators in boundary layer using a micro-manometer and a Pitot tube.

To generate AC-DBD plasma and DC-corona, following equipments are used:

1) An AC power supply with quasi-sinusoidal wave form with maximum output voltage of V=50kV, output signal maximum carrier frequency up to f_{ac}=30kHz, and maximum output power of W=1kW. A view of the equipment and a schematic of the corresponding electronic circuit are shown in Fig.4.

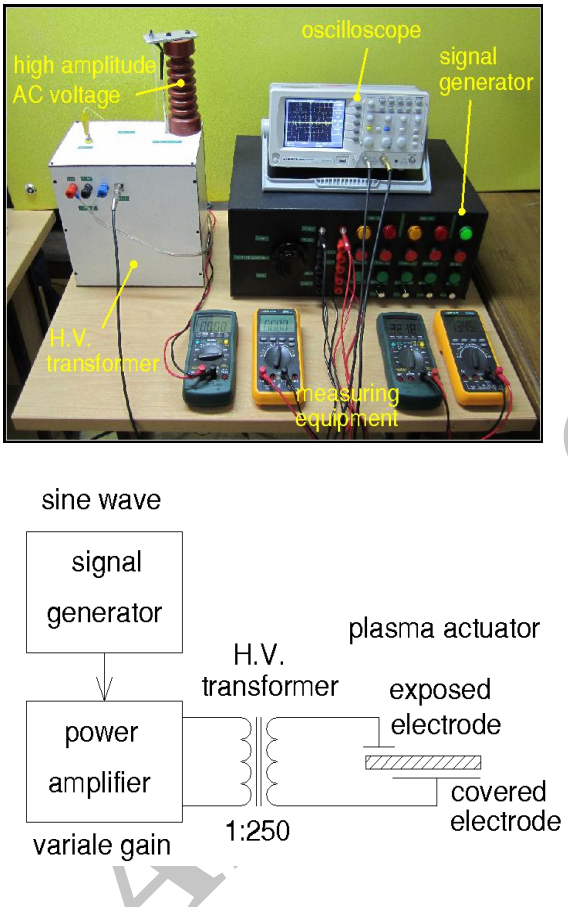

Fig. 4. AC-DBD plasma actuator and schematic view of its electronic circuit.

2) A DC power supply which uses a rectifier to produce a direct current, with maximum output voltage of V=50kV, and maximum output power of W=1kW. A view of the equipment and a schematic of the corresponding electronic circuit are shown in Fig.5.

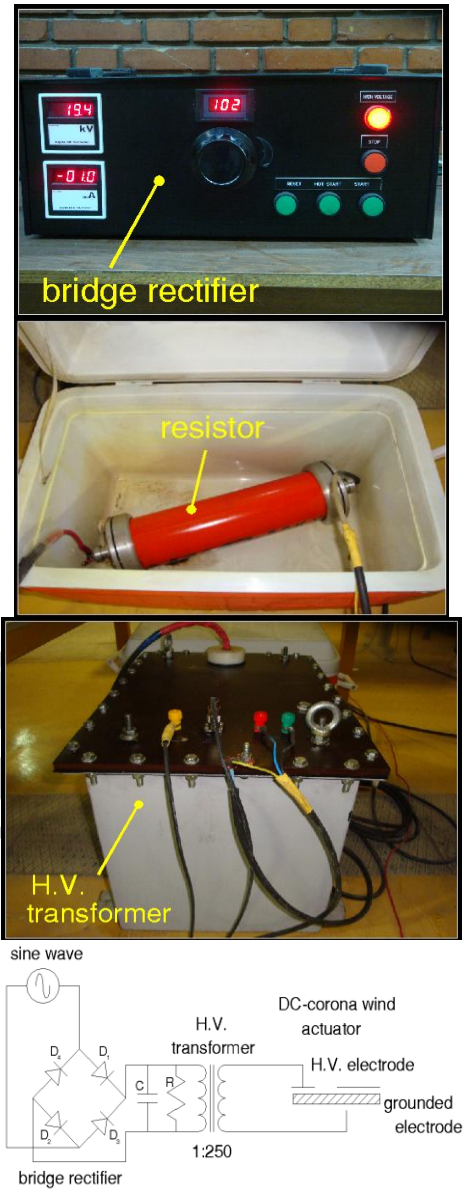

Fig. 5. DC-corona wind actuator and schematic view of its electronic circuit.

The dielectric used as insulation material for plasma generation, is a flexible Kapton adhesive with breakdown voltage of 7kV/mil (1mil=0.001 inch), the dielectric constant of 3.4 at 1MHz and thickness of 2 mil for each layer. To increase the applied voltage, 6 layers of Kapton are used. Electrodes are made from copper strips with 2 mil thickness.

The applied voltage of the AC-DBD plasma actuator is measured by a GW INSTEK GDS-1072-U digital oscilloscope. In order to measure the electric current intensity of the actuators, a series-connection of PC-interfaced True RMS DMM 4000-count digital multi-meter MS8226T in the outline of high voltage and grounded electrodes is

used. A VICTOR VC97 digital multi-meter is used to measure the AC frequency.

3.1 Visualization

In DC-corona and AC-DBD experiments, the electrodes setup is as follows:

Table 1 Geometric dimensions of the electrodes.

Plasma actuator mode --->		DC-corona	AC-DBD
Electrodes width (mm)	H.V.	5	6
	Grounded	25	12
Electrodes gap (mm)		25	0
H.V. & grounded Electrodes length (mm)		300	500

The length of the H.V. and grounded electrodes in the DC-corona and the AC-DBD are chosen to be 300mm and 500mm respectively, to guarantee a fully two dimensional flow. Because of the presence of the dielectric material between the two electrodes of the AC-DBD, they can be placed significantly closer to each other.

It is possible to observe the DC-corona wind generation in a dark room. A photograph of our experiment for the DC-corona wind is shown in Fig. 6. It is observed that the ionic wind is in the direction of the electric field. This is the path of the charged particles which migrate from the H.V. electrode to the grounded electrode. The intensity of the corona wind in sharp points is of course higher than that in other smoother points.

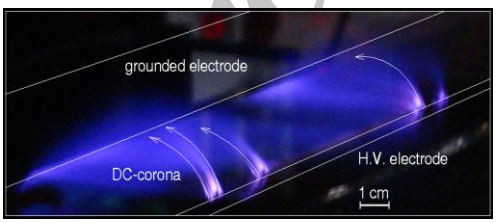

Fig. 6. DC-corona wind in the direction of electric field lines, ΔV=12kV.

To observe the particle path, smoke is slowly injected parallel to the H.V. electrode surface on the flat plate in still air. When the voltage is applied, the air particles move toward the grounded electrode so that the particle trajectories follow the electric field lines. This is clearly observed in Fig.7.

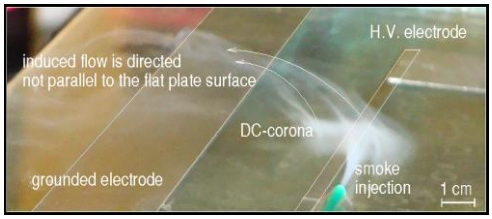

Fig. 7. Visualization of the particle path by smoke injection technique, ΔV=12kV.

The maximum strength of the DC-corona is restricted by the maximum applied voltage at which a direct electric arc does not take place. When the magnitude of the applied voltage exceeds this critical point, (here V=15kV), a direct discharge arc is occurred in weak (sharp) spots, which greatly reduces the strength of the DC-corona wind. These direct electric arcs act as conductors and consequently waste a great portion of the electric intensity. A snapshot of these arcs is shown in Fig.8.

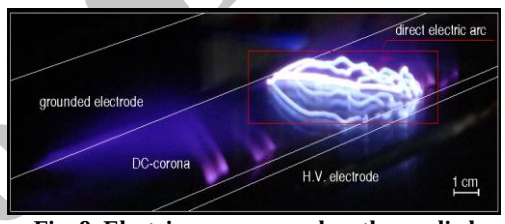

Fig. 8. Electric arc occurs when the applied voltage exceeds the critical value, ΔV=15kV.

When the dielectric layer of Kapton is applied between the electrodes, the process of electron movement from H.V. electrode to the grounded electrode is eliminated, due to the saturation of electron generation. Because the electric field is stationary, as soon as the voltage is applied, a large amount of electrons are suspended on the dielectric surface, until the dielectric surface is saturated by these electrons. The dielectric layer prevents the aggregation of these electrons on the grounded electrode surface and no particle motion is generated.

When an AC power supply is used, due to the high carrier frequency of the supplier, the permeation of the charged particles is increased. Namely, because of the high frequency of the actuation, charged particles do not have enough time to exchange their charges and thus always most of the charged particles remain in the environment for a longer period of time. The dielectric material between the electrodes causes the stability of the plasma discharge process and also prevents the heating of the electrodes. The most important property of these actuators is that they can sustain a large volume of electric discharges at atmospheric pressure without the discharge being limited to a narrow constricted electrical arc. This is governed by the build-up of charges on the dielectric surface. A photograph of

the plasma generation which is taken in our dark room is shown in Fig.9.

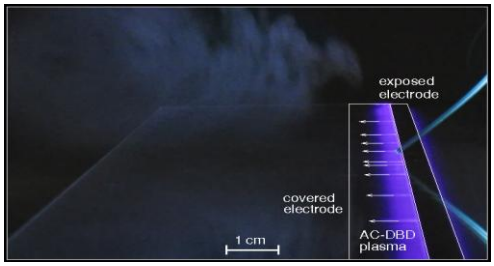

Fig. 9. A snapshot of plasma generated tangential to the flat plate surface, ΔV=9kV, f_{ac}=12kHz.

To observe the particle path, smoke is injected slowly to the covered electrode surface on the flat plate in still air. When the voltage is applied, ionized air particles move rapidly toward the grounded electrode and their trajectory is tangential to the flat plate surface. The particles sweep a path following the electric field lines, which is shown in Fig.10.

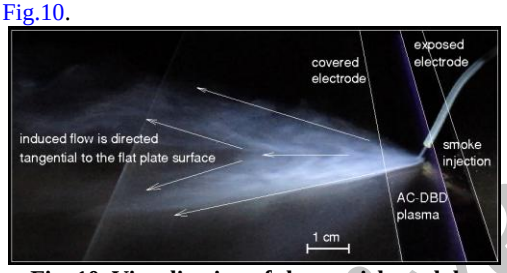

Fig. 10. Visualization of the particle path by smoke injection, ΔV=9kV, f_{ac}=12kHz.

As we discussed in section 2, although the direction of electron generation may be changed in the two half cycles of one impulse, but the direction of the net body force is always from the exposed electrode to the covered electrode. The response time of the air particles (due to the molecules inertia) is significantly slower than the response frequency of the plasma. Thus, these particles do not feel any changes in the electric field direction. Therefore they are moved in the direction of the small streaks of luminous electric discharge.

Similar to the DC-corona case, when the magnitude of applied voltage exceeds the critical voltage (here V=18kV), a direct discharge arc is observed in weak spots. This is shown in Fig.11.

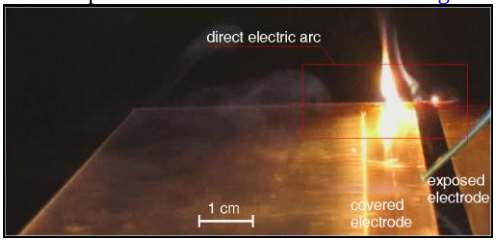

Fig. 11. Electric arc occurs in the weak points by increasing the applied voltage, ΔV=18kV.

It is evident that when an insulating dielectric is not used between the electrodes, the pure body force applied to the particles is zero. The reason for this is that the rate of electron production in two half cycles of one impulse is identical. Thus the applied forces to the fluid particles in the two half cycles by these electrons are eliminated by each other and the net body force becomes zero.

3.2 Induced Velocity Measurements

To measure the induced velocity on the flat plate, the high resolution digital micro-manometer Testo 0560 5126 with accuracy of ±0.1Pa is used. This accuracy causes ±0.05 uncertainty for the induced velocity which is a reasonable value for our measurements. The outer diameter of the Pitot tube is 0.6 mm and is located 6mm downstream the high voltage electrode and 0.3mm above the surface to measure the nearest velocity to the flat plate surface. Our measurements of the induced velocity versus applied voltage for two kind of AC-DBD and DC-corona actuation are compared in Fig.12. From Fig. 12, it is observed that by increasing the applied voltage, for the AC-DBD plasma, a maximum induced velocity is reached at about U=5m/s (for V=9kV and f_{ac}=12kHz). Then the induced velocity decreases due to the generation of high temperature streaks of luminous electric discharges. This discharge leads to partial loss of actuator power as heat, light and sound. Thus after this peak point, although the current intensity of the plasma is increased by increasing the applied voltage, but with generation and growth of the streaks of electric discharge (which act as conductors), the strength and velocity of the AC-DBD plasma is reduced. Therefore the optimal AC-DBD plasma is the purely homogenous plasma where the luminous discharge streaks are not created. An example of these streaks of luminous discharge which are made by increasing the applied voltage in constant frequency of 12 kHz is shown in Fig. 13.

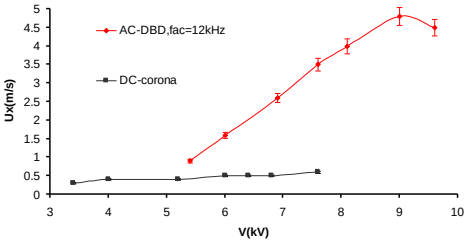

Fig. 12. Tangential induced velocity by AC-DBD and corona plasma actuators in Y=0.3mm above the flat plate surface (nearest point to the wall where Pitot tube can be installed).

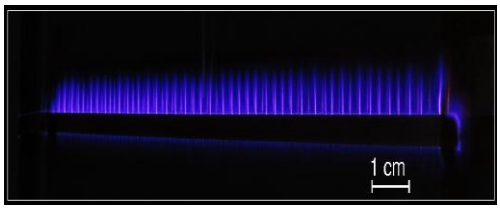

Fig. 13. Filamentary luminous discharge caused by increasing the applied voltage, f_{ac} =12 kHz, 6 layer Kapton, ΔV=15kV.

In Fig. 12, we observe that the induced velocity of the DC-corona wind increases slowly by increasing the applied voltage.

As shown in Fig.12, the induced velocity by AC-DBD plasma actuator, in the nearest point to the wall, is in the range of 5 m/s but the induced velocity by corona plasma actuator is smaller than 0.5 m/s. Therefore, the induced velocity of an AC-DBD actuator is approximately one order of magnitude greater than that of a DC-corona actuator. This difference is mainly due to the fact that for AC-DBD plasma, the direction of the charged particles is tangential to the surface, while the direction of a DC-corona wind is not tangential to the surface and has components in other directions.

Our measurements of the horizontal component of the induced velocity by both AC-DBD and DC-corona actuators versus vertical distance from the surface are shown in Fig. 14. To measure the horizontal component of the induced velocity, a micro-Pitot tube about 6mm downstream the high voltage electrode is used. The vertical motion of the tube is facilitated by connecting the micro-Pitot tube to the vertical traverse system, which moves in 0.5mm steps.

Our results in Fig.14 show that in the vicinity of the surface, the induced velocity of the AC-DBD actuator is maximized, where the induced velocity by the DC-corona actuator is approximately zero. As shown in Fig. 14 in the upper layer of the surface (Y>20mm), the induced velocity of the AC-DBD actuator vanishes rapidly. At this point (Y=20mm) the induced velocity by the DC-corona reaches a maximum of U_x~2 m/s and decreases by increasing height. From this plot, it is observed that with respect to momentum transfer, the AC-DBD is a far superior method. To be precise, we see that a large volume of air is unnecessarily affected by the DC-corona for Y>20mm, while the induction of the AC-DBD actuator is focused on the area adjacent to the wall surface with a stronger induced velocity. This pattern of flow induction renders the AC-DBD actuators to be highly suitable for the boundary layer flow control applications. In fact, Fig. 14 shows that, depending on the flow geometry, the induced velocity of the DC-corona may reach and perturb regions outside the boundary layer which can be considered an undesirable effect for most applications. This is the main difference of the AC-DBD and DC-corona actuators.

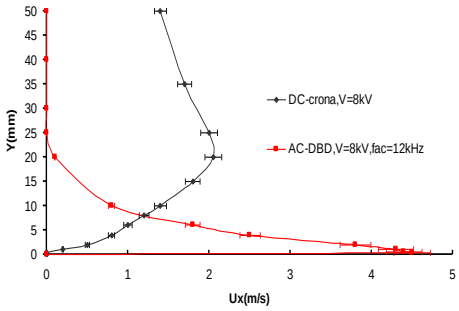

Fig. 14. The horizontal induced velocity by AC-DBD and DC-corona plasma actuators on a flat plate

4. RESULTS AND DISSCUSION

To calculate the power consumption per unit length of the electrodes for AC-DBD and DC-corona wind actuators, the following equations are used respectively:

$$W_{AC-DBD} = \frac{(V_{rms} \times I_{rms})}{L_e} = \frac{V_{pick-pick} \times I_{rms}}{2\sqrt{2}L_e} \quad (2)$$

$$W_{DC-corona} = \frac{(V_{pick} \times I_{rms})}{L_e} = \frac{V_{pick} \times I_{rms}}{L_e} \quad (3)$$

Here, to calculate the power consumption of the actuators, the electric current intensity drawn by them is also needed. For our experiments, the electric current consumption of both actuators versus applied voltage is shown in Fig. 15. This plot shows that the electric current drawn by the AC-DBD plasma actuator is higher than that of a DC-corona actuator, at the same applied voltage. This is due to the high frequency and thus high permeation of the AC-DBD plasma, which generates a spatially distributed volume of small electric discharges, as previously mentioned.

Although the electric current consumption of the AC-DBD plasma actuator is higher than the DC-corona actuator, because of the reduction factor of $1/2\sqrt{2}$ (due to the alternating nature of the actuation) in the power consumption formula, the effective power consumption per unit length of electrodes of the AC-DBD plasma is lower than the DC-corona actuator. Thus the AC-DBD plasma actuators can be more energy effective in boundary layer flow control applications.

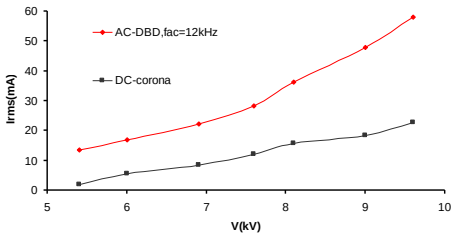

Fig. 15. Root-Mean-Square current intensity versus applied voltage for AC-DBD and DC-corona actuator.

In Fig. 16, following Eq. (2) and Eq. (3), the power consumption per unit length of electrodes of AC-DBD and DC-corona wind actuators are plotted versus the applied voltage.

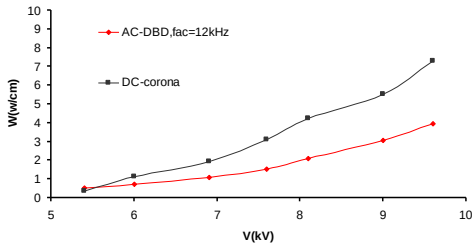

Fig. 16. Power consumption versus applied voltage for AC-DBD and DC-corona actuator.

The above visualizations and measurements show that, there is a substantial difference between the induced flow by an AC-DBD and a DC-corona actuator. The AC-DBD plasma actuators are local actuators meaning their induced velocity is confined to the actuator base. Also their induced velocity is tangential to the surface.

In the AC-DBD plasma actuators, because of the high response time of the alternating current, (f_{ac} is in the range of kHz), with every change in the signal polarity, the direction of the charged particles is also changed. Thus the motion of the charged particles is always adjacent to the wall surface and therefore the induced flow is tangential to the surface. In the DC-corona plasma actuators, however, the charged particles are always accelerated in a fixed electric field direction and consequently their induced flow has components perpendicular to the surface. This is the major difference between the two types of the plasma actuators. These differences are, schematically shown in Fig. 17.

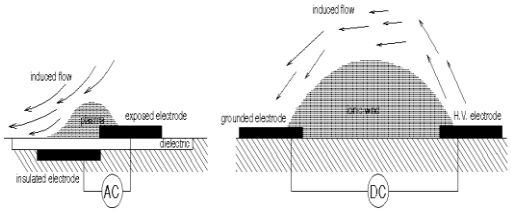

Fig. 17. The main differences between AC-DBD and DC-corona actuators in induction of flow on the flat plate.

5. CONCLUSION

Our most important results are as follows:

- An AC-DBD plasma actuator is capable of maintaining a large volume of localized electric discharges at atmospheric conditions. These discharges are not limited to a narrow region of electric discharge, as shown in Fig. 9.
- The use of the dielectric material between the electrodes, to minimize their size, is only possible when an AC input with a high frequency is applied. When the frequencies are low, the charged particles have enough time to exchange their charges. As a result, most particles of the environment become neutral and consequently cannot generate a body force. In the DC input cases, because of the fix electric field, the insulating material prevents the migration of the charged particles and no particle motion is generated.
- The AC-DBD plasma actuators are highly useful for flow control in the boundary layer, because their induced flow is tangential to the surface. Also they can be made in a smaller size which helps them to be installed in the exact necessary locations.
- The power consumption of an AC-DBD plasma actuator is desirably lower and also its induced velocity is significantly higher than that of a DC-corona wind actuator.
- The induced flow by a DC-corona actuator is oriented in the electric field direction, which is not necessarily tangential to the flat plat surface. Thus these actuators are suitable when the local shape and curvatures of the body follows the iso-curves of the applied electric filed.

ACKNOWLEDGEMENTS

This research is carried out in the Aerodynamic Research Laboratory of Department of Aerospace in K. N. Toosi University. Special appreciation goes to Masoud Mirzaei, Gholamhossein PourYousefi and Alireza Doostmahmoodi for providing support with the experimental setup. The review and comments on the manuscript by Hossein Parishani (University of Delaware) is highly appreciated.

REFERENCES

Artana, G., R. Sosa, E. Moreau, and G. Touchard (2003). Control of the near wake flow around a circular cylinder with electrohydrodynamic Actuators. *Exp. Fluids 36 (6), 580–588.*

Baughn, J. W., C. Porter, B. L. Peterson, T. E. McLaughlin, C. L. Enloe, G. I. Font, and C. Baird (2006). Momentum Transfer for an Aerodynamic Plasma Actuator with an Imposed Boundary Layer. *AIAA Paper 2006-168.*

Benard, N., P. Braud, and J. Jolibois (2008). Airflow Reattachment Along a NACA 0015 Airfoil by Surface SDBD Actuator-Time Resolved PIV Investigation. *AIAA Paper 2008-4202.*

Colver, G. and S. El-Khabiry (1999). Modeling of DC corona discharge along an electrically conductive flat plate with gas flow. *IEEE Trans. Ind. Appl. 35 (2), 387–394.*

Corke, T. and M. Post (2004). Overview of Plasma Actuators: Concepts, Optimization, and applications. *AIAA Paper, 2005-0563.*

Corke, T. C., C. He, and M. Patel (2004). Plasma Flaps and Slats: An Application of Weakly-Ionized Plasma Actuators. *AIAA Paper 2004-2127.*

Corke, T. C., Martiqua, L. Post, and D. M. Orlov (2008). Single Dielectric Barrier Discharge Plasma Enhanced Aerodynamics: Physics, Modeling and Applications. Plasma Enhanced Aerodynamics, *Review Article: Experiments in Fluids*

D'Adamo, J., G. Artana, E. Moreau, and G. Touchard (2002). Control of the airflow close to a flat plate with electrohydrodynamic actuators. *ASME-3104.*

Do, H., W. Kim, M. O. Mungal, and M. A. Cappelli (2007). Bluff Body Flow Separation Control Using Surface Dielectric Barrier Discharges. *AIAA Paper 2007-939.*

Enloe, L., T. McLaughlin, VanDyken, Kachner, E. Jumper, and T. Corke (2004). Mechanisms and responses of a single-dielectric barrier plasma actuator: *Plasma morphology. AIAA 42 , 589–594.*

Font, G. (2004). Boundary Layer Control with Atmospheric Plasma Discharges. *AIAA Paper 2004-3574.*

Font, G. and W. L. Morgan (2005). Plasma Discharges in Atmospheric Pressure Oxygen for Boundary Layer Separation Control. *AIAA Paper 2005-4632.*

Font, G. I. (2006). Boundary Layer Control with Atmospheric Plasma Discharges. *AIAA Journal*, 44(7). 1572–1578.

Forte, M., J. Jolibois, E. Moreau, G. Touchard, and M. Cazalens (2006). Optimization of a Dielectric Barrier Discharge Actuator by Stationary and Non-stationary Measurements of the Induced Flow Velocity - Application to Flow Control. *3rd AIAA Flow Control Conference, AIAA Paper* 2006-2863.

Gibalov, V. and G. Pietsch (2000). The development of dielectric barrier discharges in gas gaps and on surfaces. *J.Phys.D 33.*

Gregory, J., C. Porter, D. Sherman, and T. McLaughlin (2008). Circular Cylinder Wake Control Using Spatially Distributed Plasma Forcing. *AIAA Paper* 2008-4198.

Huang, J., T. C. Corke, and F. O. Thomas (2006). Plasma Actuators for Separation Control of Low-Pressure Turbine Blades. *AIAA Journal*, 44(1), 51–57.

Huang, J., T. C. Corke, and F. O. Thomas (2006). Unsteady Plasma Actuators for Separation Control of Low-Pressure Turbine Blades. *AIAA Journal*, 44(7), 1477–1487.

Kimmel, R. L., J. R. Hayes, J. A. Menart, and J. Shang (2004). Effect of Surface Plasma Discharges on Boundary Layers at Mach 5. *AIAA Paper. 2004-0509.*

Melcher, J. R. (1981). Continuum electromechanics. *Cambridge, Mass, MIT Press.*

Merriman, S., E. Ploenjes, P. Palm, and I. Admovich (2001). Shock Wave Control by Nonequilibrium Plasmas in Cold Supersonic

Gas Flows. *AIAA Journal,* 39(8).

Noger, C., J. S. Chang, and G. Touchard (1997). Active controls of electrohydrodynamically induced secondary flow in corona discharge reactor. *Second International Symposium on Plasma Technology in Pollution Control, Bahia, 136–141*.

Orlov, D. M. (2006). Modelling and Simulation of Single Dielectric Barrier Discharge Plasma Actuators. *PhD thesis*, University of Notre Dame.

Orlov, D., T. Corke, and M. Patel (2006). Electric Circuit Model for Aerodynamic Plasma Actuator. *AIAA Paper 2006-1206.*

Pashaie, B., S. Dhali, and F. Honea (1994). Electrical characteristics of a coaxial dielectric barrier discharge. *J. Phys. D: Applied Phys.* 27 , 2107.

Post, M. L. and T. C. Corke (2004). Separation Control on a High Angle of Attack Airfoil Using Plasma Actuators. *AIAA Journal*, 42(11), 2177–2184.

Post, M. L. and T. C. Corke (2006). Separation Control Using Plasma Actuators—Dynamic Stall Vortex Control on an Oscillating Airfoil. *AIAA Journal,* 44(12), 3125–3135.

Rizzetta, D. and M. Visbal (2008). Large-Eddy Simulation of Plasma-Based Control Strategies for Bluff Body Flow. *AIAA Paper 2008-4197.*

Roth, J. R. and D. Sherman (2000). Electrohydrodynamic flow control with a glow discharge surface plasma. *AIAA J.* 38 (7) 1166–1178.

Roth, J. R. (2003). Aerodynamic Flow Acceleration Using Paraelectric and Peristaltic Electrohydrodynamic Effects of a One Atmosphere Uniform Glow Discharge Plasma. *Physics of Plasmas*, 10(5). 2117–2126.

Samimy, M., I. Adamovich, B. Webb, J. Kastner, J. Hileman, S. Keshav, and P. Palm (2004). Development and Characterization of Plasma Actuators for High Speed Jet Control. *Experiments in Fluids*,37(4), 577–588 .

Schatzman, D. and F. O. Thomas (2008). Turbulent Boundary Layer Separation Control Using Plasma Actuators. *AIAA Paper 2008-4199.*

Seyed-Yagoobi, J. and J. E. Bryan (1981). Enhancement of heat transfer and mass transport in single-phase and two-phase flows with electrohydrodynamics. *Texas A&M University College Station Texas, 77843-3123.*

Sosa, R., E. Moreau, G. Touchard, and G. Artana (2004). Stall control of airfoils at high angle of attack with periodically excited EHD actuators. *AIAA Paper No. 2004-2738.*

Suchomel, C., D. Van Wie, and D. Risha (2003). Perspectives on Cataloguing Plasma Technologies Applied to Aeronautical Sciences. *AIAA Paper, 2003-3852.*

Thomas, F. O., A. Kozlov, and T. C. Corke (2005). Plasma Actuators for Landing Gear Noise Control. *AIAA Paper 2005-3010.*

Thomas, F. O., A. Kozlov, and T. C. Corke (2008). Plasma Actuators for Cylinder Flow Control and Noise Reduction. *AIAA Journal,* 46(8), 1921–1931.

Van Ness, D. K., T. C. Corke, and S. C. Morris (2006). Turbine Tip Clearance Flow Control Using Plasma Actuators. *AIAA Paper 2006-0021.*

Wilkinson, S. P. (2003). Investigation of an oscillating surface plasma for turbulent drag reduction. *AIAA Paper No. 2003-1023*